DEVELOPMENT OF FREE VORTEX WAKE METHOD FOR AERODYNAMIC LOADS ON ROTOR BLADES

Hamidreza Abedi[*], Lars Davidson[*], Spyros Voutsinas[**]

[*](Division of Fluid Dynamics, Department of Applied Mechanics, Chalmers University of Technology, Göteborg, Sweden)

[**](Fluid Section, School of Mechanical Engineering, National Technical University of Athens, Athens, Greece)

[*]e-mail: abedih@chalmers.se, lada@chalmers.se

[**]e-mail: spyros@fluid.mech.ntua.gr

Abstract

Among clean energy sources that are renewable, wind is regarded as the least destructive to the environment. According to data provided by the Renewables Global Status Report in 2013, wind capacity increased globally by 19% per year, the increase being 45 GW. That is, it reached 283 GW to a record high despite the uncertainty in the policy in the key markets. By the exponential growth of wind turbines all around the world, and its general acceptance among people, the demand and its worthwhileness makes it apt for research, especially to enhance its performance.

The aerodynamics of a wind turbine is governed by the flow around the rotor, where the prediction of air loads on rotor blades in different operational conditions and its relation to rotor structural dynamics is crucial for design purposes. One of the most important challenges in wind turbine aerodynamics is therefore to accurately predict the forces on the blade, where the blade and wake are modeled by different approaches such as the Blade Element Momentum (BEM) theory, the vortex method and Computational Fluid Dynamics (CFD).

A free vortex wake method, based on the potential, inviscid and irrotational flow, is developed to study the aerodynamic loads. The results are compared with the BEM [1] method, the GENUVP [2] code and CFD [3] (see also the acknowledgments).

Keyword: aerodynamic load, rotor blade, wind turbine, lifting line, lifting surface, vortex lattice method, free wake.

Introduction

The methods for predicting wind turbine performance are similar to propeller or helicopter theories. There are different methods for modelling the aerodynamics of a wind turbine with different levels of complexity and accuracy, such as the BEM theory and solving the Navier-Stokes equations using CFD.

Today, engineering methods based on the BEM method are used extensively for analyzing the aerodynamic performance of a wind turbine. The BEM model is based on the steady and homogeneous flow assumption and that aerodynamic loads act on an actuator disc instead of a finite number of blades.

The BEM method is computationally fast and is easily im-

1

plemented, but it is acceptable only for a certain range of flow conditions [1]. A number of empirical and semi-empirical correction factors have been added to the BEM in order to increase its application range, such as yaw misalignment, dynamic inflow, dynamic stall, tower influence, finite number of blades and blade cone angle [4], but they are not relevant to all operating conditions and are often incorrect at high tip speed ratios where wake distortion is significant [5].

The vortex theory, which is based on the potential, inviscid and irrotational flow can also be used to predict the aerodynamic performance of wind turbines. It has been widely used for aerodynamic analysis of airfoils and aircrafts. Although the standard method cannot be used to predict viscous phenomena such as drag and boundary layer separation, its combination with tabulated airfoil data makes it a powerful tool for the prediction of fluid flow. Compared with the BEM method, the vortex method is able to provide more physical solutions for attached flow conditions using boundary layer corrections, and it is also valid over a wider range of turbine operating conditions. Although it is computationally more expensive than the BEM method, it is still feasible as an engineering method.

In vortex methods, the trailing and shed vortices are modeled by either vortex particles or vortex filaments moving either freely, known as free wake [2,6,7] or restrictedly by imposing the wake geometry, known as prescribed wake [8,9]. The prescribed wake requires less computational effort than the free wake, but it requires experimental data to be valid for a broad range of operating conditions. The free wake model, which is the most computationally expensive vortex method, is able to predict the wake geometry and loads more accurately than the prescribed wake because of less restrictive assumptions.

Finally, CFD, which solves the Navier-Stokes equations for the flow around the rotor blade, is known as the most accurate but computationally most expensive method making it an impractical engineering method for wind turbine applications, at least with the current computational hardware resources.

The aim of this paper is to study the application of vortex method for wind turbine load calculation. A developed time-marching vortex lattice free wake is used for the simulation and the predictions are compared with the other approaches mentioned above.

Theory

Vortex flow theory is based on assuming incompressible ($\nabla \cdot \overrightarrow{V} = 0$) and irrotational ($\nabla \times \overrightarrow{V} = 0$) flow at every point except at the origin of the vortex, where the velocity is infinite [10]. A region containing a concentrated amount of vorticity is called a vortex, where a vortex line is defined as a line whose tangent is parallel to the local vorticity vector everywhere. Vortex lines surrounded by a given closed curve make a vortex tube with a strength equal to the circulation Γ. A vortex filament with a strength of Γ, is represented as a vortex tube of an infinitesimal cross-section with strength Γ.

According to the Helmholtz theorem, an irrotational motion of an inviscid fluid which started from rest remains irrotational. Also, a vortex line cannot end in the fluid. It must form a closed path, end at a solid boundary or go to infinity; this implies that vorticity can only be generated at solid boundaries. Therefore, a solid surface may be considered as a source of vorticity. Hence the solid surface in contact with fluid is replaced by a distribution of vorticity.

For an irrotational flow, a velocity potential, Φ, can be defined as $\overrightarrow{V} = \nabla\Phi$, where in order to find the velocity field, the Laplace's equation, $\nabla^2\Phi = 0$, is solved using a proper boundary condition for the velocity on the body and at infinity. In addition, in vortex theory, the vortical structure of a wake can be modeled by either vortex filaments or vortex particles, where a vortex filament is modeled as concentrated vortices along an axis with a singularity at the center. The velocity induced by a straight vor-

tex filament can be determined by the Biot-Savart law as

$$\overrightarrow{V}_{ind} = \frac{\Gamma}{4\pi} \frac{\overrightarrow{dl} \times \overrightarrow{r}}{\mid \overrightarrow{r} \mid^3} \qquad (1)$$

which can also be written as

$$\overrightarrow{V}_{ind} = \frac{\Gamma}{4\pi} \frac{(r_1 + r_2)(\overrightarrow{r}_1 \times \overrightarrow{r}_2)}{(r_1 r_2)(r_1 r_2 + \overrightarrow{r}_1 \cdot \overrightarrow{r}_2)} \qquad (2)$$

where Γ denotes the strength of the vortex filament and $\overrightarrow{r_1}$, $\overrightarrow{r_2}$ are the distance vectors from the beginning, A, and end, B, of a vortex segment to an arbitrary point C, respectively (see fig.(1)).
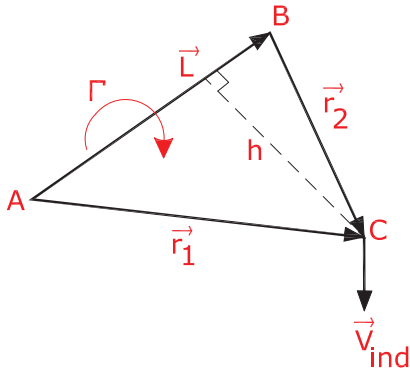
FIGURE 1.   Schematic for the Biot-Savart law

The Biot-Savart law has a singularity when the point of evaluation (C) of induced velocity is located on the vortex filament axis ($\overrightarrow{L}$). Also, when the evaluation point is very near to the vortex filament, there is an unphysically large induced velocity at that point. The remedy is either to use a cut-off radius, δ [11], or to use a viscous vortex model with a finite core size by multiplying a factor to remove the singularity [12].

The Biot-Savart law correction based on the viscous core correction model can be made by introducing a finite core size, r_c, for a vortex filament [13]. There are two general approaches representing the induced velocity using the desingularized algebraic profile, i.e., a constant viscous core size which is used

extensively in engineering applications because of its simplicity and a diffusive viscous core size where the core size grows with time based on the Lamb-Oseen model [13].

A general form of a desingularized algebraic swirl-velocity profile for stationary vortices is proposed by Vasitas [14] as

$$V_\theta(r) = \frac{\Gamma}{2\pi}\left(\frac{r}{(r_c^{2n} + r^{2n})^{1/n}}\right) \qquad (3)$$

Bagai [15] suggested the velocity profile based on eq.(3) for $n = 2$ for the rotor tip vortices. Therefore, in order to take into account the effect of viscous vortex core, a factor of K_v must be added to the Biot-Savart law as [15]

$$\overrightarrow{V}_{ind} = K_v \frac{\Gamma}{4\pi} \frac{(r_1 + r_2)(\overrightarrow{r}_1 \times \overrightarrow{r}_2)}{(r_1 r_2)(r_1 r_2 + \overrightarrow{r}_1 \cdot \overrightarrow{r}_2)} \qquad (4)$$

where

$$K_v = \frac{h^n}{(r_c^{2n} + h^{2n})^{1/n}} \qquad (5)$$

and h is defined as the perpendicular distance of the evaluation point (see fig.(1)). Factor K_v desingularizes the Biot-Savart equation when the evaluation point distance tends to zero and prevents a high induced velocity in the vicinity region of the vortex core radius.

Assumptions

Each engineering model is constructed based on some assumptions. Here, some of those are discussed. The upstream flow is set to be uniform, both in time and space, and it is perpendicular to the rotor plane (parallel to the rotating axis). However, it can be either uniform or non-uniform (varying both in time and space). Blades are assumed to be rigid, so the elastic effect of the blades is neglected. Also, because of the large circulation gradients ($d\Gamma/dr$) near the tip and the root of the rotor blade, it

is suggested to use the cosine rule for the blade radial segmentation [4] where the blade elements, in the spanwise direction, are distributed at equi-angle increments.

In the vortex lattice free wake model, a finite number of vortex wake elements move freely based on the local velocity field, and contrary to the prescribed wake model, allowing wake expansion as well. Each vortex wake element contains two points, one at the head (A), and another at the tail (B) (see fig.(1)), which are known as Lagrangian markers, where the induced velocity components are calculated using the Biot-Savart law; their movements give rise the wake deformation. The vortex flow theory assumes that the trailing and shed wake vortices extend to infinity. However, since the effect of the induced velocity field by the far wake is small on the rotor blade, the wake in the present study extends only to three or four diameters downstream of the wind turbine rotor plane.

Vortex Lattice Free Wake (VLFW)
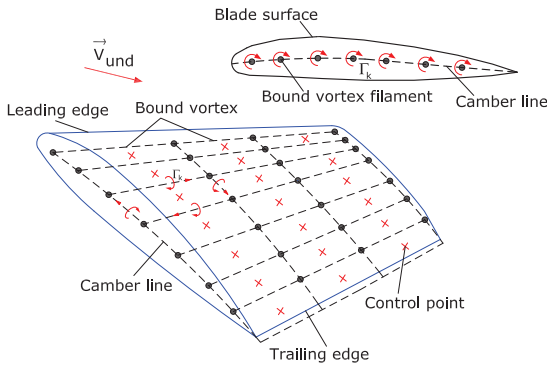
FIGURE 2.   Lifting surface and vortex panels construction

The vortex lattice method (VLM) is based on the thin lifting surface theory of vortex ring elements [16], where the blade surface is replaced by vortex panels that are constructed based on the airfoil camber line of each blade section (see fig.(2)). The solution of Laplace's equation with a proper boundary condition

gives the flow around the blade resulting in an aerodynamic load calculation, generated power and thrust of the wind turbine. In
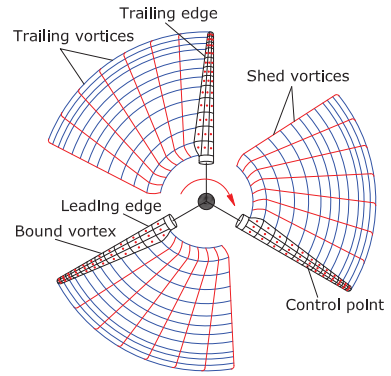

FIGURE 3.   Schematic of vortex lattice free wake

order to take into account the blade surface curvature, the lifting surface is divided into a number of panels both in the chordwise and spanwise directions, where each panel contains vortex ring with strength $\Gamma_{i,j}$ in which i and j indicate panel indices in the chordwise and spanwise directions, respectively. The strength of
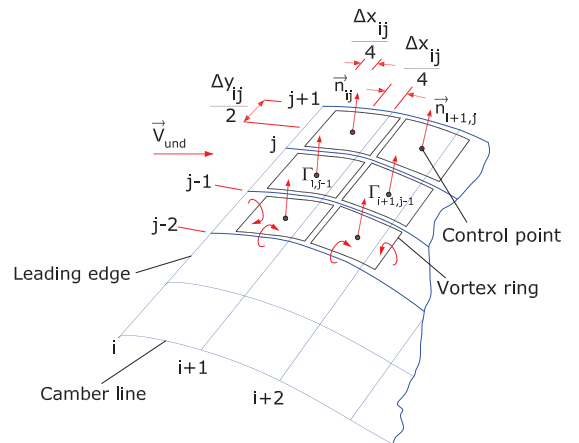

FIGURE 4.   Numbering procedure

each blade bound vortex ring element, $\Gamma_{i,j}$, is assumed to be constant over the panel and the positive circulation is defined on the

basis of right-hand rotation rule. In order to fulfill the 2D Kutta condition (which can be expressed as $\gamma_{T.E.} = 0$ in terms of the strength of the vortex sheet) the leading segment of a vortex ring is located at the 1/4 panel length (see fig.(4)). The control point of each panel is located at 3/4 of the panel length meaning that the control point is placed at the center of the panel's vortex ring. Generally, the wake vortices are modeled as vortex ring elements that are trailed and shed, based on the time-marching method, from the trailing edge; in the wake they induce a velocity field around the blade. To find the blade bound vortices' strength, the flow tangency condition at each blade control point must be specified by establishing a system of equations. Therefore, the normal vector at each control point must be defined (see fig.(4)). The velocity components at each blade control point includes the free stream ($\overrightarrow{V}_{\infty}$), rotational ($\Omega\overrightarrow{r}$), blade vortex rings self-induced ($\overrightarrow{V}_{ind,bound}$) and wake induced ($\overrightarrow{V}_{ind,wake}$) velocities. The blade induced component is known as influence coefficient a_{ij} and is defined as the induced velocity of a jth blade vortex ring with a strength equal to one on the ith blade control point. If the blade is assumed to be rigid, then the influence coefficients are constant at each time step, which means that the left-hand side of the equation system is computed only once. However, if the blade is modeled as a flexible blade, they must be calculated at each time step. Since the wind and rotational velocities are known during the wind turbine operation, they are transferred to the right-hand side of the equation system. In addition, at each time step, the strength of the wake vortex panels is known from the previous time step, so the induced velocity contribution by wake panels is also transferred to the right-hand side. Therefore, the system of equations can be expressed as

$$\begin{pmatrix} a_{11} & a_{12} & \cdots & a_{1m} \\ a_{21} & a_{22} & \cdots & a_{2m} \\ \vdots & \vdots & \ddots & \vdots \\ a_{m1} & a_{m2} & \cdots & a_{mm} \end{pmatrix} \begin{pmatrix} \Gamma_1 \\ \Gamma_2 \\ \vdots \\ \Gamma_m \end{pmatrix} = \begin{pmatrix} RHS_1 \\ RHS_2 \\ \vdots \\ RHS_m \end{pmatrix} \quad (6)$$

where m is defined as $m = M \times N$ for a blade with an M spanwise and an N chordwise panels and the right-hand side is computed as

$$RHS_k = -\left(\overrightarrow{V}_{\infty} + \Omega\overrightarrow{r} + \overrightarrow{V}_{ind,wake}\right)_k \cdot \overrightarrow{n}_k \quad (7)$$

The blade bound vortex strength ($\Gamma_{i,j}$) is calculated by solving eq.(6) at each time step. At the first time step (see fig.(5) and (6)),
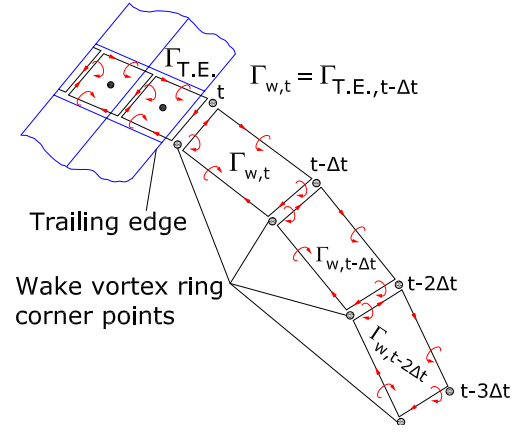

FIGURE 5. Schematic of generation and moving of wake panels at each time step

there are no free wake elements. At the second time step (see fig.(5) and (7)), when the blade is rotating, the first wake panels are shed. Their strength is equal to the bound vortex circulation of the last row of the blade vortex ring elements (Kutta condition), located at the trailing edge, at the previous time step (see fig.(5)), which means that $\Gamma_{W_{t_2}} = \Gamma_{T.E.,t_1}$, where the W and $T.E.$ subscripts represent the wake and the trailing edge, respectively. At the second time step, the strength of the blade bound vortex rings is calculated by specifying the flow tangency boundary condition where, in addition to the blade vortex ring elements, the contribution of the first row of the wake panels is considered.

This methodology is repeated, and the vortex wake elements are trailed and shed at each time step, where their strengths

remain constant (Kelvin theorem) and their corner points are moved based on the governing equation (eq.(8)) by the local velocity field, including the wind velocity and the induced velocity by all blade and wake vortex rings (see fig.(6) and (7)). The
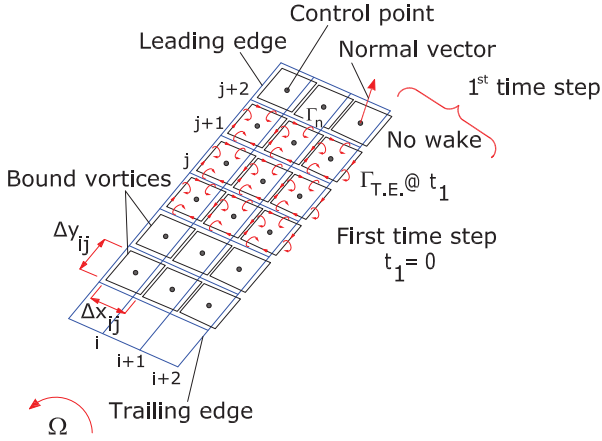

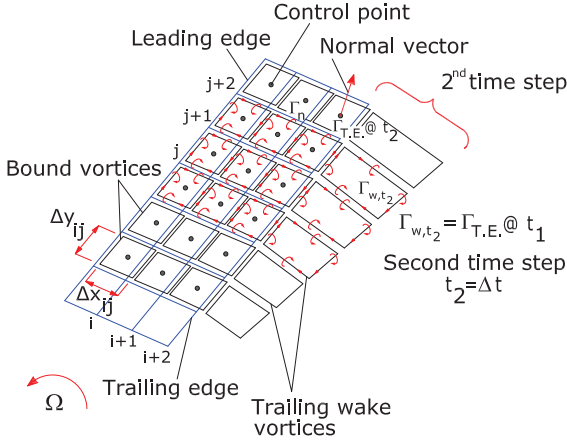**FIGURE 6**. Schematic of wake evolution at the first time step

FIGURE 7. Schematic of wake evolution at the second time step

governing equation for the wake geometry is

$$\frac{d\overrightarrow{r}}{dt} = \overrightarrow{V}(\overrightarrow{r}, t) \qquad \overrightarrow{r}(t = 0) = \overrightarrow{r_0} \qquad (8)$$

where $\overrightarrow{r}$, $\overrightarrow{V}$ and t denote the position vector of a Lagrangian marker, the total velocity field and time, respectively, and the total velocity field, expressed in the rotating reference frame i.e., $\overrightarrow{V}_{rot} = 0$, can be written as

$$\overrightarrow{V} = \overrightarrow{V}_{\infty} + \overrightarrow{V}_{ind,blade} + \overrightarrow{V}_{ind,wake} \qquad (9)$$

Different numerical schemes may be used for eq.(8) such as the explicit Euler method, the implicit method, the Adams-Bashforth method and the Predictor-Corrector method. The numerical integration scheme must be considered in terms of the accuracy, stability and computational efficiency. Here, the first-order Euler explicit method is used as

$$\overrightarrow{r}_{t+1} = \overrightarrow{r}_t + \overrightarrow{V}(\overrightarrow{r}_t)\Delta t \qquad (10)$$

where $\overrightarrow{V}$ is taken at the old time step.

In each time step, when the position of all the Lagrangian markers is calculated, we are able to compute the velocity field around the rotor blade where, as a consequence, the lift force can be calculated according to the Kutta-Jukowski theorem which in differential form reads as

$$\overrightarrow{dL} = \rho\overrightarrow{V} \times \Gamma\overrightarrow{dl} \qquad (11)$$

where ρ, $\overrightarrow{V}$, Γ and $\overrightarrow{dl}$ denote air density, velocity vector, vortex filament strength and length vector, respectively. The Kutta-Jukowski theorem is applied at the mid point of the front edge of each blade vortex ring and gives the potential lift force where the lift force of each spanwise blade section is calculated by summing up the lift force of all panels along the chord. The lift force for each blade panel except the first row near the leading edge is computed by

$$\overrightarrow{L}_{i,j} = \rho\overrightarrow{V}_{tot,i,j} \times (\Gamma_{i,j} - \Gamma_{i-1,j})\Delta\overrightarrow{y}_{i,j} \qquad (12)$$

and, for the blade panels adjacent to the leading edge, eq.(12) can be written as

$$\overrightarrow{L}_{1,j} = \rho \overrightarrow{V}_{tot,1,j} \times \Gamma_{1,j} \Delta \overrightarrow{y}_{1,j} \qquad (13)$$

where $\overrightarrow{V}_{tot,i,j}$ is computed as

$$\overrightarrow{V}_{tot,i,j} = \overrightarrow{V}_{und,i,j} + \overrightarrow{V}_{ind,wake,i,j} + \overrightarrow{V}_{ind,bound,i,j} \qquad (14)$$

The total lift of each blade section in the spanwise direction can be written as

$$\overrightarrow{L}_j = \sum_{i=1}^{N} \overrightarrow{L}_{i,j} \qquad (15)$$

where N denotes the number of spanwise sections. Decomposition of the lift force for each blade spanwise section into the normal and tangential directions with respect to the rotor plane (see fig.(8)) gives the effective angle of attack for each section.

$$\alpha = tan^{-1} \left(F_t / F_n \right) - \theta_t - \theta_p \qquad (16)$$

where α, F_t, F_n, θ_t and θ_p represent the effective angle of attack, tangential force, normal force, blade section twist and blade pitch, respectively. The generated power and thrust are determined by the tangential and normal forces, respectively.
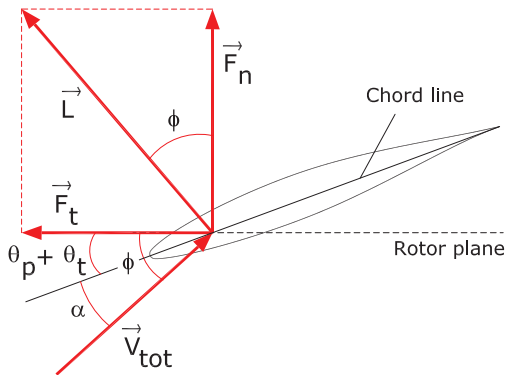
FIGURE 8.   Potential load decomposition

Model	Power [MW]	Thrust [kN]	Time [hr]
VLFW	1.96	347.82	3
CFD	1.70	477.08	750
BEM	1.92	373.15	7E-5
GENUVP	1.90	365.28	5.6

TABLE 1.   Power and Thrust for the different methods

Results and Conclusions

The results of the vortex lattice free wake model (VLFW) are compared with the BEM method, GENUVP code and CFD. In the vortex method simulations made with VLFW and GENUVP, the blade is discretized with 25 spanwise sections (see fig.(9)) with fine tip resolution and 8 equally spaced chordwise sections. 10 degrees in the azimuthal direction is employed for the wake segmentation and the wake length is truncated after 4 rotor diameter. It is assumed that the wake vortex filament core radius is constant and is equal to $1[m]$. The CFD simulation made by [3] using a RANS (Reynolds-Averaged Navier-Stokes) solver. The 5MW reference wind turbine [17] is used in the simulations and the operation conditions are $\overrightarrow{V}_\infty = 8.0 \, [m/s]$ and $\Omega = 0.954$ $[rad/s]$ as the uniform, steady free stream and the constant rotational velocity, respectively.
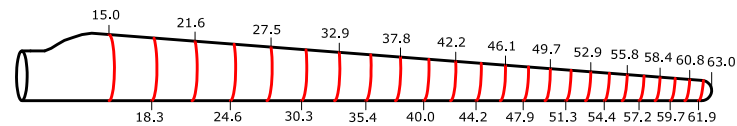

FIGURE 9.   Radial distribution of blade elements

Table (1) shows a comparison between the four different methods. Since the vortex method (VLFW and GENUVP) is a potential flow (no viscous drag), it predicts more power than

7

the BEM and CFD methods.

The simulation time difference between the VLFW and CFD is significant which means that the VLFW method may be known as a reduced order model for wind turbine load calculations standing between the BEM and CFD methods both in accuracy and time efficiency.
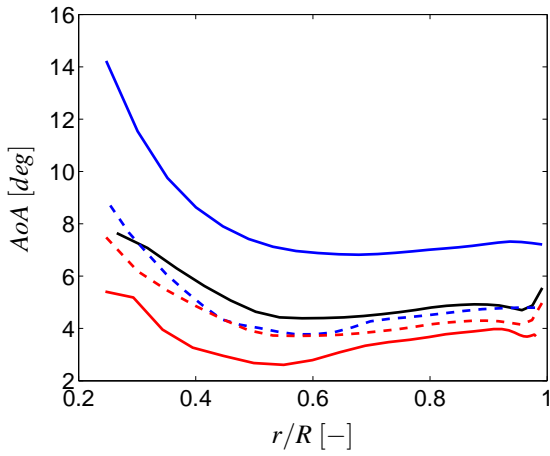

FIGURE 10. Distribution of the angle of attack (geometric and effective) along the blade, ———: *Geom*, ———: *CFD*, ———: *VLFW*, ------: *BEM*, ------: *GENUVP*

Figure (10) shows the geometric and the effective angle of attack along the blade. As can be seen, in all cases, because of the induced velocity field around the rotor blade, the effective angle of attack is less than the geometric one, which makes a significant power reduction for a wind turbine. Therefore, prediction of the induced velocity field around the rotor blade generated by the wake and the blade vortex ring elements is the key point for the vortex flow solution.

Figure (11) shows the tangential force ($\overrightarrow{F_t}$) with respect to the rotor plane. Near the blade tip, the tangential force for all methods is larger than near the blade root, which means that the tip region of the blade produces more power compared with the other parts of the blade, especially the root region. As we know,
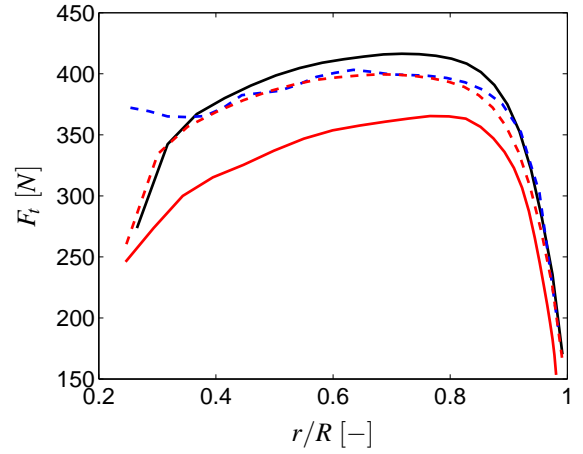
FIGURE 11. Distribution of the tangential force along the blade, ———: *CFD*, ———: *VLFW*, ------: *BEM*, ------: *GENUVP*

the generated power of a wind turbine is computed on the basis of the tangential force. Hence, according to fig.(11), it is concluded that the VLFW method, as a potential flow, must predict the more power compared to the other methods, whereas the CFD, as a viscous flow, must produce less power than the others. This fact is verified by looking at table (1).
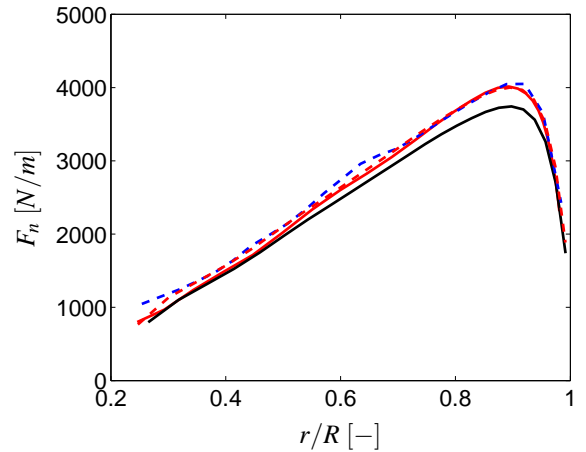

FIGURE 12. Distribution of the normal force along the blade, ———: *CFD*, ———: *VLFW*, ------: *BEM*, ------: *GENUVP*

The normal force ($\overrightarrow{F_n}$) along the blade is shown in fig.(12)

which, similar to the tangential force, near the blade tip, it is much larger than at the blade root. As can be seen, the agreement is good between the different methods. However, the VLFW model predicts less normal force in comparison with the CFD and the other methods. It can be concluded that neglecting the viscosity effect (as in the vortex flow) increases the tangential and decreases the normal force.

References

[1] Hansen, M. O., 2008. *Aerodynamics Of Wind Turbines*. 2nd edition, EarthScan.

[2] Voutsinas, S., 2006. "Vortex Methods In Aeronautics: How To Make Things Work". *International Journal of Computational Fluid Dynamics, 20*, pp. 3–18.

[3] Shen, W. Z., October 9-11, 2012. "Study of tip loss corrections using CFD rotor computations". In The Science of Making Torque from Wind Conference, Oldenburg, Germany.

[4] van Garrel, A., August 2003. *Development Of A Wind Turbine Aerodynamics Simulation Module*. ECN report, ECN-C–03-079.

[5] Vermeer, L., Sørensen, J., and Crespo, A., 2003. "Wind Turbine Wake Aerodynamics". *Progress in Aerospace Sciences, 39*, pp. 467–510.

[6] Gupta, S., 2006. *Development Of A Time-Accurate Viscous Lagrangian Vortex Wake Model For Wind Turbine Applications*. University of Maryland, Department of Aerospace Engineering.

[7] Pesmajoglou, S., and Graham, J., 2000. "Prediction Of Aerodynamic Forces On Horizontal Axis Wind Turbines In Free Yaw And Turblence". *Journal of Wind Engineering and Industrial Aerodynamics, 86*, pp. 1–14.

[8] Chattot, J., 2007. "Helicoidal Vortex Model For Wind Turbine Aeroelastic Simulation". *Computers and Structures, 85*, pp. 1072–1079.

[9] Chattot, J., 2003. "Optimization Of Wind Turbines Using Helicoidal Vortex Model". *Journal of Solar Energy Engineering, 125*, pp. 418–424.

[10] Anderson, J., 2001. *Fundamentals Of Aerodynamics*, 3rd ed. McGraw-Hill.

[11] van Garrel, A., 2001. *Requirements For A Wind Turbine Aerodynamics Simulation Module*, 1st ed. ECN report, ECN-C-01-099.

[12] Leishman, J., and Bagai, M. J., 2002. "Free Vortex Filament Methods For The Analysis Of Helicopter Rotor Wakes". *Journal of Aircraft,* **39**.

[13] Bhagwat, M., and Leishman, J., 2002. "Generalized Viscous Vortex Model For Application To Free-Vortex Wake and Aeroacoustic Calculations". In 58th Annual Forum and Technology Display of the American Helicopter Society International.

[14] Vasitas, G., Kozel, V., and Mih, W., 1991. "A Simpler Model For Concentrated Vortices". *Experiments in Fluids,* **11**, pp. 73–76.

[15] Bagai, A., and Leishman, J., 1993. "Flow Visualization Of Compressible Vortex Structures Using Density Gradient Techniques". *Experiments in Fluids,* **15**, pp. 431–442.

[16] Katz, J., and Plotkin, A., 2001. *Low-Speed Aerodynamics*, 2nd ed. Cambridge University Press.

[17] Jonkman, J., Butterfield, S., Musial, W., and Scott, G., 2009, NREL/TP-500-38060. *Definition Of A 5-MW Reference Wind Turbine For Offshore System Development*. National Renewable Energy Laboratory, Colorado, USA.